A multidisciplinary approach to landslide monitoring in the Arctic: Case study of the March 2018 ML 1.9 seismic event near the Karrat 2017 landslide

Kristian Svennevig*[1], Anne Munck Solgaard[1], Sara Salehi[1], Trine Dahl-Jensen[1], John Peter Merryman Boncori[2], Tine B. Larsen[1] and Peter H. Voss[1]

RESEARCH ARTICLE | OPEN ACCESS
GEUS Bulletin Vol 43 | e2019430208 | Published online: 01 July 2019
https://doi.org/10.34194/GEUSB-201943-02-08

The landslide of 17 June 2017 at Karrat Fjord, central West Greenland, triggered a tsunami that caused four fatalities. The catastrophe highlighted the need for a better understanding of landslides in Greenland and initiated a recent nation-wide landslide screening project led by the Geological Survey of Denmark and Greenland (GEUS; see also Svennevig (2019) this volume).

This paper describes an approach for compiling freely available data to improve GEUS' capability to monitor active landslides in remote areas of the Arctic in near real time. Data include seismological records, spaceborne Synthetic Aperture Radar (SAR) data and multispectral optical satellite imagery. The workflow was developed in 2018 as part of a collaboration between GEUS and scientists from the Technical University of Denmark (DTU). This methodology provides a model through which GEUS will be able to monitor active landslides and provide relevant knowledge to the public and authorities in the event of future landslides that pose a risk to human life and infrastructure in Greenland.

We use a minor event on 26 March 2018, near the site of the Karrat 2017 landslide, as a case study to demonstrate 1) the value of multidisciplinary approaches and 2) that the area around the landslide has continued to be periodically active since the main landslide in 2017.

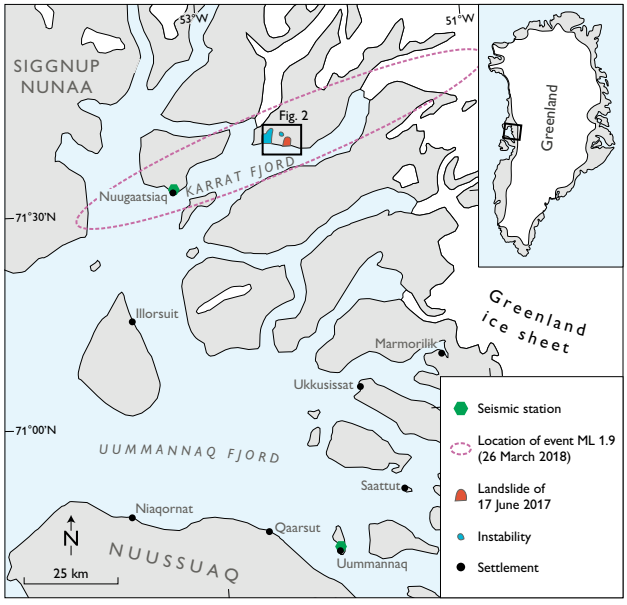

Fig. 1 Overview map of the Uummannaq Fjord area showing the location of the 26 March 2018 1.9 ML seismic event (ellipse) along with the position of the 17 June 2017 landslide at Karrat and the nearby instabilities. The size of the landslide and nearby instabilities are slightly exaggerated for clarity on the small map scale. Seismic stations in Uummannaq and Nuugaatsiaq are shown along with settlements in the area.

Geological setting and description of the landslide area

The geology of the Karrat area (Fig. 1) predominantly consists of reworked Archaean gneiss interfolded with supracrustal rocks of the Palaeoproterozoic Karrat Group (Henderson & Pulvertaft 1967). Locally, around the landslide and surrounding unstable areas, the succession consists of Archaean gneiss overlain by Palaeoproterozoic semipelitic to pelitic schist. The geology of the Karrat 2017 landslide has not been mapped in detail; however, an ongoing mapping project aims to update the geological maps of the area (e.g. Sørensen & Guarnieri 2018).

During the landslide of 17 June 2017, 35–58 million m^3 of material were mobilised (Bessette-Kirton *et al.* 2017; Gauthier *et al.* 2018). A preliminary examination of the Karrat 2017 landslide shows that a number of precursor events took place in the years prior to the main landslide. Unstable areas that may fail in the future have also been identified. Of these, two principal areas (marked with Y and Z in Fig. 2A) west of the scarp of the main slide (marked by 'X' in Fig. 2A)

show signs of significant deformation both before and after the 2017 landslide. This activity is observable in both optical satellite images and in the results derived from remotely sensed Differential Synthetic Aperture Radar (SAR) Interferometry (DInSAR; Y and Z in Figs 2A, D, E).

Data

The various data sources used here have different temporal and spatial resolutions. Individually, they provide unique information for landslide monitoring, but their value increases significantly when combined. As such, integration of data from seismograms, DInSAR and optical images can provide a more complete understanding of the geological processes contributing to landslide activity.

Seismic events

The present Greenland Ice Sheet Monitoring Network (GLISN) of seismographs consists of 21 stations, situated about 200 km or more apart (Clinton *et al.* 2014). Given this large distance, the uncertainty associated with the horizontal location of detected earthquakes or other types of seismic events in Greenland can be up to 50 km.

Differentiation of tectonic and non-tectonic events is based on the judgement of an experienced seismologist. For example, the main seismic features associated with tectonic earthquakes are clearly separated body waves, higher frequency content and a well-located hypocentre at depth, whereas non-tectonic events are not dominated by higher frequencies. These can be caused in several ways. Glacial events, such as those caused by calving ice, have an epicentre located near an outlet glacier and often contain a low frequency component (Ekström *et al.* 2003; Nettles *et al.* 2008). Large landslides can also generate seismic signals, but these are often of longer duration than those caused by tectonic earthquakes, such as the seismic signals caused by the 2000 Paatuut (Dahl-Jensen *et al.* 2004) and the 2017 Karrat (Clinton *et al.* 2017) landslides. For smaller landslide events (e.g. events without catastrophic failure and rock avalanche activity), the duration will be shorter and the amplitude smaller, and it may be difficult to distinguish them with seismic data alone from other non-tectonic seismic sources, e.g. signals generated by moving sea ice or glaciers. Integration of other data sources are thus necessary.

Optical satellite images

Sentinel-2A and -2B are multispectral optical satellite imaging systems that cover 13 spectral bands at various spatial resolutions: 4 bands at 10 m resolution (including visual light), 6 bands at 20 m and 3 bands at 60 m. The revisit frequency of Sentinel-2A and -2B over the Karrat Fjord area is 1–2 days at around 15:30–16:00 UTC (12:30–13:00 local time). However, no images are collected between the end of October and the start of March as it is too dark. The present study is limited to visual interpretation of Sentinel-2 images as change detection algorithms have not been implemented.

DInSAR

DInSAR (Rosen *et al.* 2000) was applied to Sentinel-1A and Sentinel-1B synthetic aperture radar (SAR) data acquired between 24 February and 13 April 2018. This method provides one-dimensional ground motion measurements in the satellite line-of-sight direction, i.e. towards and away from the radar. The main acquisition mode of Sentinel-1 over land is the Interferometric Wide (IW) swath mode, which provides 250 km × 250 km images at a 5 m × 20 m spatial resolution in the ground range and flight-path directions, respectively. The Karrat area is covered by two satellite tracks: descending track 25 and ascending track 90. However, on ascending passes in track 90, the area of interest slopes towards the radar, leading to significant radar foreshortening (and in some locations even to layover). In turn, this causes geometric decorrelation of the radar signal even for small interferometric baselines, due to the horizontal spreading of the scatterers within each resolution cell (i.e. due to the poor line-of-sight resolution). For this reason, we used data from track 25 only in this analysis.

Unlike optical data from e.g. Sentinel-2, SAR has the advantage of being insensitive to cloud cover and solar illumination, and imagery can therefore be acquired year-round. DInSAR can be applied to data collected along the same radar track, which are available every six days for the Sentinel-1A/B constellation on the Greenland ice sheet margin. One of the main requirements of DInSAR is a sufficient level of coherence (i.e. statistical similarity) between the two acquisitions. In practice, this limits the number of good interferograms collected during the winter season, as snowfall may change the surface morphology between two acquisitions and cause loss of coherence. For this study, both 6 and 12 day differential interferograms were constructed. Topographic contributions to the interferometric phase were removed using ArcticDEM version 2.0 (Porter *et al.* 2018) and additional corrections (courtesy of E.V. Sørensen, GEUS) were

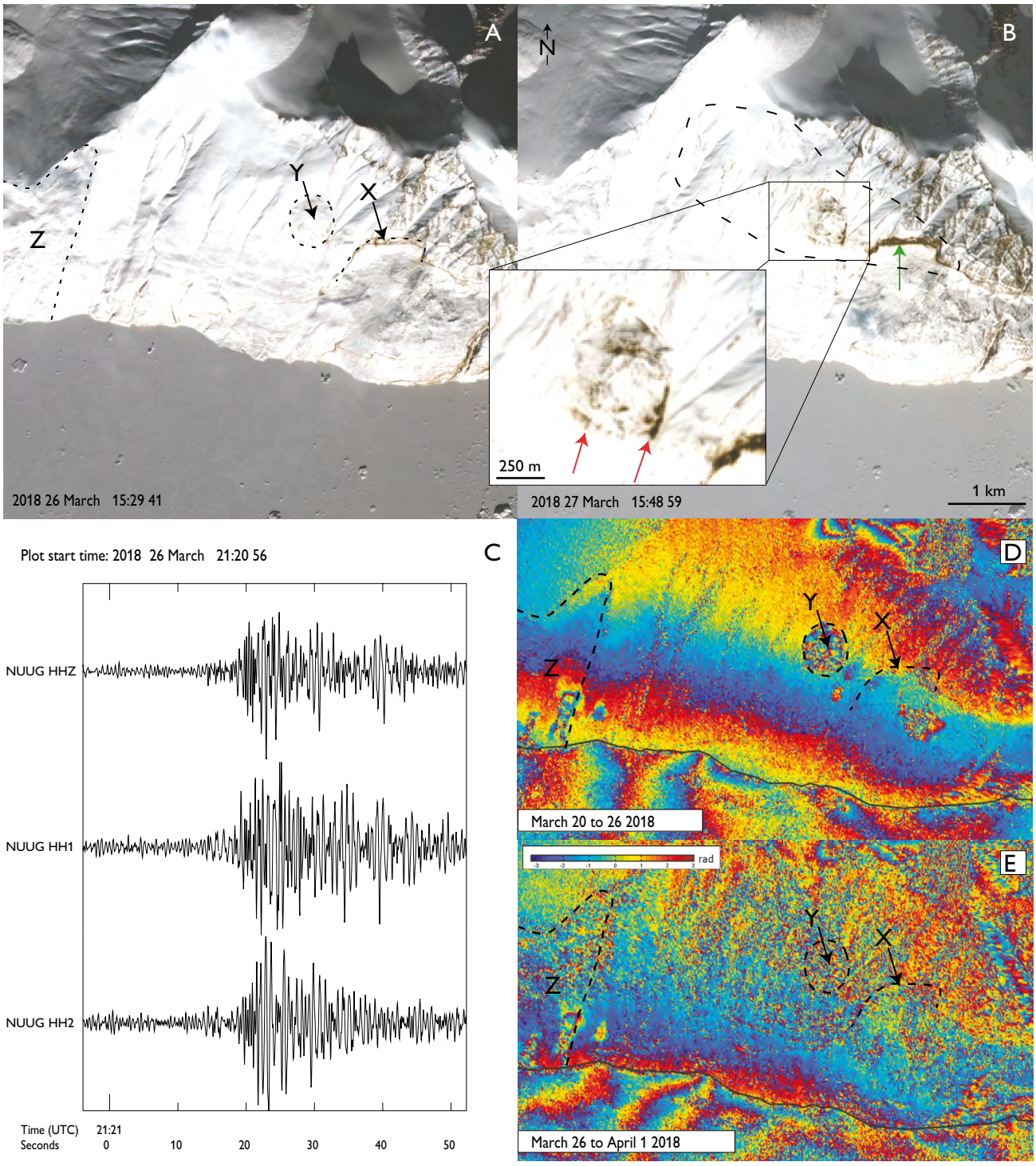

Fig. 2 Composite figure with the different datasets used to constrain the event. **A**: Sentinel-2A RGB image from 26 March 2018 15:29 41 UTC. Dashed line at **X** shows the scar of the 17 June 2017 landslide and **Y** shows the outline of the active area to the SW. **Z** indicates the position of a large older landslide with periodic activity in the toe. **B**: Sentinel-2B RGB image from 27 March 2018 15:48 59 UTC. Red arrows show rock fall at the unstable area Y and the green arrow shows rock fall at the back scarp of the Karrat 2017 event. The dotted black line shows the outline of the area affected by the event, as observed in the inset image. **C**: The 26 March 2018 21:21 UTC 1.9 ML seismic event as recorded on the Nuugaatsiaq seismograph (Fig. 1). **D**: Sentinel-1 differential interferogram from before the event, (20180320-20180326), the latter interferogram was acquired only hours prior to the event. X, Y and Z refer to the same areas in A. **E**: Sentinel-1 differential interferogram spanning the event from (20180326-20180401). X, Y and Z refer to the same areas in A.

made to account for the height variations associated with the June 2017 landslide.

The 26 March 2018 ML 1.9 event

On 26 March 2018 at 21:21 UTC (18:21 local West Greenland time) a shallow, low frequency non-tectonic ML 1.9 seismic event was recorded on several seismographs in West Greenland (Figs 1, 2C; see the earlier discussion of tectonic vs. non-tectonic event features). The event was located to an ellipsoid of *c*. 100 by 20 km covering an area of known landslide activity near the 2017 Karrat landslide. The time between the P and S wave arrivals corresponded to the distance between the seismic station in Nuugaatsiaq, and the Karrat Landslide area. The ellipsoid also encompassed two glacial outlets (Fig. 1). To investigate the source of the seismic signal, we acquired Sentinel-2A and 2B images from 26 March 15:29 UTC and 27 March 15:48 UTC. Comparison of the two images show dark colouration of the snow (Fig. 2B) indicating rock fall from the known active area (red arrows in Fig. 2B) and the whole length of the headscarp of the Karrat 2017 landslide (green arrow in Fig 2B). The rock fall was only observed very locally on the coast and a screening of neighbouring slopes and glacial outlets showed no changes between the two images. Temperatures were well below freezing during the whole period. Images from the week before and after the event were also screened and showed no increased rock fall activity.

In the period leading up to the event, the 6 day pairs of SAR images are coherent in the whole slope area, and the differential interferograms show activity constrained to the 2017 landslide area and areas Y and Z to the west (Fig. 2). These areas, or subareas within them, show incoherence in all studied interferograms back to the spring of 2015. An example of this is given in Fig. 2D where the last image in the pair is from just hours prior to the seismic event. The image pairs (both 6 and 12 day) spanning the seismic event have a low coherence, resulting in noisy interferograms (Fig. 2E). Inspection of optical images from approximately the same time as the SAR images suggests that the observed loss of coherence is due to changes in snow cover over most of the slope likely due to redistribution by wind. It is thus not possible to observe this event in the interferograms as, for example, an increase in decorrelated area of the continuous active areas. Instead, we have to rely on observations from the optical imagery for interpretation. This emphasises the importance of using multiple independent methods for observing landslides.

Possible cause of the event

It is clear that the localised rock fall occurred across the time span of the shallow ML 1.9 non-tectonic seismic event. However, the interferograms spanning this event are noisy and thus we cannot yet confirm the exact cause of the event. However, by compiling all three independent datasets together, we suggest that landslide movement along a fracture could have generated the seismic signal and triggered localised rock fall near the epicentre. The landslide movement could have been either a rapid acceleration in creep of the unstable area west of the 2017 Karrat landslide scar (Y in Fig. 2A), or the propagation of an unknown fracture related to landslide activity – potentially the westward migration of the fracture that forms the headscarp of the 2017 landslide – or both. This appears to be supported by the fact that no catastrophic mass wasting was observed in the Sentinel-2 images, which might otherwise have indicated that the event was a true landslide like the 2017 Karrat landslide. Moreover, no large-scale calving events were observed in the two nearby glacial outlets, suggesting that glacial activity was not the cause of the seismic event. The differential interferogram prior to the event (Fig. 2D) shows that areas on the slope were moving before the event, but there are no seismic signals present during this period. Other similar seismic and rock fall events have been observed episodically throughout 2018 and eyewitnesses have reported activity in the area since the 2017 Karrat landslide took place. The area continues to be active.

Outlook

The approach described here has the potential to serve as a model contingency plan to gather the relevant information in the event of a landslide. This information could then be disseminated to the public and relevant authorities in the form of express reports.

These methods can also be applied to quantify the temporal evolution of past landslides using archive data. Sentinel-2 images are available from mid-2015 and for older events, more coarse-scale Landsat images can be used back to the early seventies. Sentinel-1A SAR data are available from October 2014, whereas both Sentinel-1A and 1B data are available from October 2016. The current GLISN seismic network is available back to summer 2010 (Clinton *et al.* 2017). The first stations were installed in Greenland in 1928, and until the 1990s the network consisted of only 3–4 stations, increasing to 5–8 stations before the GLISN network. Prior to 2010, only very large landslides would have been observed by the seismic stations, for example the 2000 Paatuut landslide (Dahl-Jensen *et al*. 2004), which also coincided with

a research network station deployment (Dahl-Jensen *et al.* 2003).

A similar approach could also be implimented to quantify activity in other remote areas that are prone to landslides. An obvious candidate is the south coast of the Nuussuaq peninsular where several catastrophical historical and prehistorical landsides are known to have occurred (Pedersen *et al.* 2002; Dahl-Jensen *et al.* 2004; Svennevig 2019).

In the future, a denser network of seismographs on a regional scale would greatly improve our capability to locate earthquakes in the area more precisely and help us to determine the cause of non-tectonic events. For example, an event that is far from a glacier terminus is less likely to be caused by glacial activity. A local seismic network around the landslide coast at Karrat would further help to determine the cause of these earthquakes by pinpointing exactly where on the slope they occur relative to known structures. A similar network could also be applied to the Vaigat coast where non-tectonic seismic events are also suspected to be caused by landslide activity, and where there is a historical record of landslides (Pedersen *et al.* 2002; Dahl-Jensen *et al.* 2004). Automation of the SAR and optical data processing (change detection; e.g., Lacroix *et al.* 2018) could also aid the workflow.

While we are unable to precisely identify the cause of the ML 1.9 seismic event, it is clear that the combination of the various datasets is key to understanding the process involved in such events and demonstrates the benefit of a multidisciplinary approach.

Acknowledgments

We thank the reviewers, Andrée Blais-Stevens and Erin Bessette-Kirton, whose comments and suggestions improved the manuscript.

References

Bessette-Kirton, E., Allstadt, K., Pursley, J. & Godt, J. 2017: Preliminary Analysis of Satellite Imagery and Seismic Observations of the Nuugaatsiaq Landslide and Tsunami, Greenland. https://www.usgs.gov/natural-hazards/landslide-hazards/science/preliminary-analysis-satellite-imagery-and-seismic?qt-science_center_objects=0#qt-science_center_objects.

Clinton, J.F. *et al.* 2014: Seismic Network in Greenland Monitors Earth and Ice System. Eos, Transactions American Geophysical Union **95**, 13-14. https://doi.org/10.1002/2014eo020001

Clinton, J., Larsen, T.B., Dahl-Jensen, T., Voss, P.H. & Nettles, M. 2017: Seismic observations from Nuugatsiaq slide/tsunami. IRIS Special event page. https://ds.iris.edu/ds/nodes/dmc/specialevents/2017/06/22/nuugaatsiaq-greenland-landslide-and-tsunami/#seismic-observations-from-nuugatsiaq-slidetsunami

Dahl-Jensen, T. *et al.* 2003: Depth to Moho in Greenland: Receiver Function Analysis suggests two Proterozoic Blocks in Greenland. Earth and Planetary Science Letters **205**, 379-393. https://doi.org/10.1016/s0012-821x(02)01080-4

Dahl-Jensen, T. *et al.* 2004: Landslide and tsunami 21 November 2000 in Paatuut, West Greenland. Natural Hazards **31**, 277–287. https://doi.org/10.1023/b:nhaz.0000020264.70048.95

Ekström, G., Nettles, M. & Abers, A.G. 2003: Glacial earthquakes. Science **302**, 622–624. https://doi.org/ 10.1126/science.1088057

Gauthier, D., Anderson, S.A., Fritz, H.M. & Giachetti, T. 2018: Karrat Fjord (Greenland) tsunamigenic landslide of 17 June 2017: initial 3D observations. Landslides **15**, 327–332. https://doi.org/10.1007/s10346-017-0926-4

Henderson, G. & Pulvertaft, T.C.R. 1967: The stratigraphy and structures of the Precambrian rocks of the Umanak area, West Greenland. Meddelelser Dansk Geologisk Forening **17**, 1–20.

Lacroix, P., Bièvre, G., Pathier, E., Kniess, U. & Jongmans, D. 2018: Use of Sentinel-2 images for the detection of precursory motions before landslide failures. Remote Sensing of Environment **215**. 507–516. https://doi.org/10.1016/j.rse.2018.03.042

Nettles, M. *et al.* 2008: Step-wise changes in glacier flow speed coincide with calving and glacial earthquakes at Helheim Glacier, Greenland. Geophysical Research Letters **35**, 1–5. https://doi.org/10.1029/2008gl036127

Pedersen, S.A.S., Larsen, L.M., Dahl-Jensen, T., Jepsen, H.F., Krarup, G., Nielsen, T., Pedersen, A.K., Von Platen-Hallermund, F. & Weng, W.L. 2002: Tsunami-generating rock fall and landslide on the south coast of Nuussuaq , central West Greenland. Geology of Greenland Survey Bulletin **191**, 73–83.

Porter, C. *et al.* 2018: ArcticDEM V2, https://doi.org/10.7910/DVN/OHHUKH, Harvard Dataverse.

Rosen, P.A., Hensley, S., Joughin, I.R., Li, F.K., Madsen, S.N., Rodriguez, E. & Goldstein, R. 2000: Synthetic aperture radar interferometry. Proc. of the IEEE **88**, 333–382. https://doi.org/10.1109/5.838084

Sørensen, E.V. & Guarnieri, P. 2018: Remote geological mapping using 3D photogrammetry: an example from Karrat, West Greenland. Geological Survey of Denmark and Greenland Bulletin **41**, 63–66.

Svennevig, K. 2019: Preliminary landslide mapping in Greenland. Geological Survey of Denmark and Greenland Bulletin **43**, e2019430207. https://doi.org/10.34194/GEUSB-201943-02-07

How to cite

Svennevig, K. Solgaard, A.M., Salehi, S., Dahl-Jensen, T., Merryman Boncori, J.P., Larsen T.B., & Voss, P.H. 2019: A multidisciplinary approach to landslide monitoring in the Arctic: Case study of the March 2018 ML 1.9 seismic event near the Karrat 2017 landslide. Geological Survey of Denmark and Greenland Bulletin **43**, e2019430208. *https://doi.org/10.34194/GEUSB-201943-02-08*

*Corresponding author: Kristian Svennevig | *E-mail: ksv@geus.dk*

[1] *Geological Survey of Denmark and Greenland (GEUS), Øster Voldgade 10, DK-1350, Copenhagen K, Denmark.*

[2] *DTU Space, National Space Institute, Technical University of Denmark, Ørsteds Plads, 2800 Lyngby, Denmark.*